Meccanica manuscript No.
(will be inserted by the editor)

Computational approach to design face-milled spiral bevel gear drives with favorable conditions of meshing and contact

Alfonso Fuentes-Aznar and Ramon Ruiz-Orzaez and Ignacio Gonzalez-Perez

Received: date / Accepted: date

Abstract The micro-geometry of the tooth surfaces of spiral bevel and hypoid pinions has to be fine-adjusted to obtain enhanced meshing and contact characteristics during the meshing process with their corresponding mating gears. In this paper, a new methodology is proposed to design face-milled spiral bevel gear drives to, firstly, derive favorable orientation and dimensions of the contact pattern between the mating surfaces of the gears and, secondly, obtain a predesigned parabolic function of negative transmission errors with limited magnitude of maximum transmission errors. The proposed approach is based on the definition of the desired topography for the active surfaces of the pinion followed by a numerical derivation of their finishing machine-tool settings through a bound-constrained optimization algorithm. Increasing mechanical strength and reducing the levels of noise and vibration of face-milled spiral bevel gear drives constitute the main objectives of the proposed design process. A numerical example is provided to illustrate the applicability of the developed theory.

Keywords Gear geometry, face-milled spiral bevel gears, finishing-cutting, gear surface topography, bound-constrained optimization

1 Introduction

Spiral bevel gear drives are applied in a wide field of applications for power transmission between intersected axes, basically due to its uniform and quiet performance together with high load carrying capacity [1–4]. Gear industry is demanding new design methodologies of this type of gear drives to increase the load carrying capacity and power-to-weight ratio, reduce levels of noise and vibration, absorb gear misalignments and increase durability and mechanical efficiency.

Derivation of machine-tool settings involved in finishing operations of mating members of both spiral bevel and hypoid gear drives has been the main objective of many research works during the last two decades. Local synthesis was probably the first proposed technique to be part of an integrated computerized approach for optimal design of low-noise adjusted bearing contact face-milled spiral bevel gear drives. It lets derive the pinion finishing machine-tool settings providing predesigned contact characteristics at a chosen contact point belonging to the driven active surface of the gear member of the gear set [2,3,5]. In [6], the introduction of a modified radial motion (MRM) as supplemental

Alfonso Fuentes-Aznar
Department of Mechanical Engineering, Rochester Institute of Technology (RIT), USA, E-mail: afeme@rit.edu

Ramon Ruiz-Orzaez
Department of Mechanical Engineering, Polytechnic University of Cartagena (UPCT), Spain, E-mail: rro0@alu.upct.es

Ignacio Gonzalez-Perez
Department of Mechanical Engineering, Polytechnic University of Cartagena (UPCT), Spain, E-mail: ignacio.gonzalez@upct.edu

flank correction motion to improve the adjustability of contact pattern in face-milled spiral bevel gear drives was proposed. Some approaches based on the definition of a predesigned ease-off topography were presented in [7–9]. In [10–13], mathematical nonlinear optimization algorithms were used with the aim of identifying finishing machine-tool settings for the manufacturing of spiral bevel and hypoid pinions provided with enhanced mechanical properties: optimal contact pattern, minimum level of peak-to-peak transmission errors and maximum mechanical efficiency. In [14,15], analytical procedures of derivation of finishing machine-tool settings corresponding to face-milled or face-hobbed spiral and hypoid bevel gears from their blank geometries were proposed.

Different methods of correction of finishing machine-tool settings corresponding to both spiral bevel and hypoid gears have been also proposed. In [2,16–19], the aforementioned methods were based on the information provided by a coordinate measuring machine (CMM), and took into account the tooth surface errors originated from machining dynamic behavior and machine-tool tolerances.

In this work, a computational approach for the numerical determination of finishing machine-tool settings corresponding to the pinion member of fixed-settings face-milled spiral bevel gear drives is proposed. It is based on the definition of an objective geometry that takes into account a predesigned function of transmission errors and the desired contact pattern, therefore following predesigned topographies of the objective surfaces. A numerical example will show the effectiveness of the proposed procedure of design of face-milled spiral bevel gears.

2 Basic ideas of the developed approach

The developed approach is based on the following ideas:

- The gear member of the spiral bevel gear set is considered as given. The machine-tool settings for the gear can be obtained from an existing summary of machine-tool settings or theoretically obtained by the approach presented in [14,15]. For that, the blank data can be obtained by following the procedure presented in ANSI/AGMA 2005-D03 [20] and ANSI/AGMA ISO 23509-A08 [21].
- The pinion member will be obtained considering the mating gear as generating tool. In the process of generation of the pinion, a predesigned function of transmission errors of a limited maximum value will be considered to meet the conditions of a low noise and vibration gear drive.
- The potential contact lines between the pinion and gear will be determined. Those potential contact lines will be modified to provide a localized contact pattern in the desired direction. By considering the deviations obtained during the process of modification of the potential contact lines, an objective topography for the contacting surfaces of the pinion is obtained.
- Finally, by using a bound-constrained optimization algorithm, the machine-tool settings corresponding to the closest manufacturable pinion tooth surfaces are obtained.

Each of the previous items is a step in the proposed procedure of design and will be further described in the following sections.

3 Geometry of the spiral bevel gear

As mentioned above, the geometry of the gear member of the gear set is considered as given. Essentially, the gear tooth surfaces are generated computationally as the envelope to the family of positions of a spread-blade face-milling cutter represented in coordinate system $S_g\left(x_g, y_g, z_g\right)$, fixed to the spiral bevel gear. Consequently, these surfaces are expressed mathematically by means of a system of nonlinear equations given by Equation (1), which is comprised of a vectorial equation (family of generating surfaces in coordinate system $S_g\left(x_g, y_g, z_g\right)$) and a scalar equation (equation of meshing). In Equation (1), variables s and θ constitute the two surface parametric coordinates associated to any point P belonging to the spread-blade face-milling cutter generating surfaces, ψ_g represents the generalized parameter of rotation associated to the generation process of the gear and matrix $\mathbf{M}_{gt}\left(\psi_g\right)$

represents the coordinate transformation from coordinate system $S_t\,(x_t, y_t, z_t)$, fixed to the cutter, to coordinate system $S_g\,(x_g, y_g, z_g)$, fixed to the being-generated gear.

$$\mathbf{r}_g(s,\theta) \equiv \begin{cases} \mathbf{r}_g\,(s,\theta,\psi_g) = \mathbf{M}_{gt}(\psi_g)\mathbf{r}_t(s,\theta) \\ f_g\,(s,\theta,\psi_g) = \left(\frac{\partial \mathbf{r}_g(s,\theta,\psi_g)}{\partial s} \times \frac{\partial \mathbf{r}_g(s,\theta,\psi_g)}{\partial \theta}\right) \cdot \frac{\partial \mathbf{r}_g(s,\theta,\psi_g)}{\partial \psi_g} = 0 \end{cases} \tag{1}$$

A detailed description of the computerized generation of face-milled spiral bevel gear drives can be found in [2,3,5].

4 Generation of the pinion by its mating gear

The second stage of the proposed approach consists on the computational generation of the pinion. The active tooth surfaces of the pinion are derived analytically using the active tooth surfaces of the gear as generating surfaces under a predefined rolling condition to achieve a predesigned function of transmission errors.

4.1 Applied coordinate systems

Figure 1 shows the applied coordinate systems for generation of the pinion, as well as simulation of meshing and tooth contact analysis (TCA). A brief description of the coordinate systems is as follows:

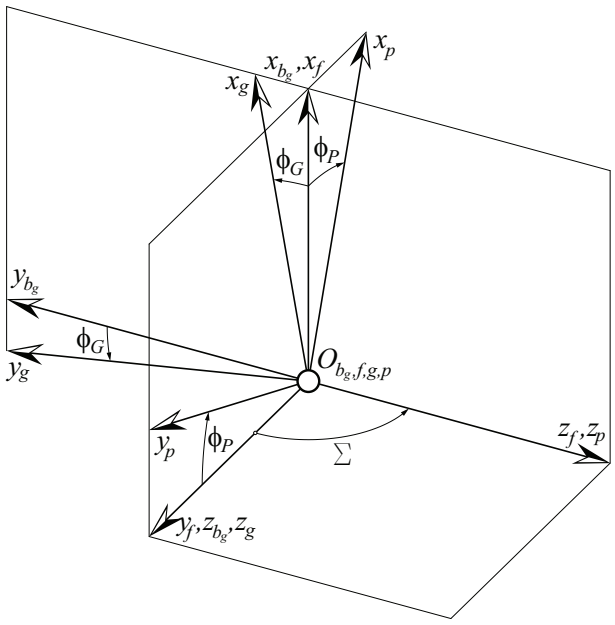

Fig. 1 Applied coordinate systems applied for generation of the pinion.

- $S_f\,(x_f, y_f, z_f)$. This is the fixed coordinate system, and it is rigidly connected to the frame.
- $S_p\,(x_p, y_p, z_p)$. This movable coordinate system is attached to the pinion. The pinion rotation axis coincides with the axis z_p, which is collinear with axis z_f, and its origin O_p is located on the pinion pitch cone apex.
- $S_g\,(x_g, y_g, z_g)$. This movable coordinate system is attached to the gear. The gear rotation axis coincides with the axis z_g, and its origin O_g is located on the gear pitch cone apex.

– $S_{b_g}\left(x_{b_g}, y_{b_g}, z_{b_g}\right)$. This auxiliary coordinate system is rigidly connected to fixed coordinate system S_f, and it lets to simulate the shaft angle Σ.

Angles ϕ_P and ϕ_G are the rotation angles of pinion and gear, respectively.

4.2 Geometry of the pinion tooth surfaces

The parametric representation of the family of the gear generating surfaces in coordinate system $S_p\left(x_p, y_p, z_p\right)$ generated by the mating gear active surface $\mathbf{r}_g(s,\theta)$ (Eq. (1)) is given by

$$\mathbf{r}_p\left(s,\theta,\phi_P,\phi_G\right) = \mathbf{M}_{pg}\left(\phi_P,\phi_G\right)\mathbf{r}_g\left(s,\theta\right) \tag{2}$$

with matrix $M_{pg}(\phi_P,\phi_G)$ being the coordinate transformation from coordinate system $S_g(x_g,y_g,z_g)$, fixed to the spiral bevel gear, to coordinate system $S_p(x_p,y_p,z_p)$, fixed to the spiral bevel pinion, and given by (see Figure 1)

$$\mathbf{M}_{pg}\left(\phi_P,\phi_G\right) = \mathbf{M}_{pf}\left(\phi_P\right)\mathbf{M}_{fb_g}\mathbf{M}_{b_g g}\left(\phi_G\right) \tag{3}$$

Here,

$$\mathbf{M}_{pf}\left(\phi_P\right) = \begin{bmatrix} \cos\phi_P & -\sin\phi_P & 0 & 0 \\ \sin\phi_P & \cos\phi_P & 0 & 0 \\ 0 & 0 & 1 & 0 \\ 0 & 0 & 0 & 1 \end{bmatrix} \tag{4}$$

$$\mathbf{M}_{fb_g} = \begin{bmatrix} 1 & 0 & 0 & 0 \\ 0 & \cos\Sigma & \sin\Sigma & 0 \\ 0 & -\sin\Sigma & \cos\Sigma & 0 \\ 0 & 0 & 0 & 1 \end{bmatrix} \tag{5}$$

$$\mathbf{M}_{b_g g}\left(\phi_G\right) = \begin{bmatrix} \cos\phi_G & -\sin\phi_G & 0 & 0 \\ \sin\phi_G & \cos\phi_G & 0 & 0 \\ 0 & 0 & 1 & 0 \\ 0 & 0 & 0 & 1 \end{bmatrix} \tag{6}$$

Figure 2 shows the theoretical process of generation of a spiral bevel pinion by its mating spiral bevel gear.

The equation of meshing for generation of the spiral bevel pinion by its mating gear allows the envelope to the family of generating gear tooth surfaces to be obtained and it is expressed in differential geometry [2] by

$$f_p\left(s,\theta,\phi_P,\phi_G\right) = \left(\frac{\partial \mathbf{r}_P\left(s,\theta,\phi_P,\phi_G\right)}{\partial s} \times \frac{\partial \mathbf{r}_P\left(s,\theta,\phi_P,\phi_G\right)}{\partial \theta}\right) \cdot \frac{\partial \mathbf{r}_P\left(s,\theta,\phi_P,\phi_G\right)}{\partial \phi_P} = 0 \tag{7}$$

The angle of rotation of the pinion, ϕ_P, is considered the generalized parameter of rotation associated to the generating process.

4.3 Predesigning a parabolic function of transmission errors

According to the second stage of the proposed approach, the angles of rotation of pinion and gear, given by parameters ϕ_P and ϕ_G in Eq. (7), will follow a modified roll polynomial function to provide the gear set with a predesigned parabolic function of transmission errors. The use of polynomial functions as motion curves provides several advantages in both hypoid and spiral bevel gear drives to reduce noise and vibration by absorbing the almost-linear discontinuous functions of transmissions errors caused by misalignments and reducing tooth mesh impacts during the process of load transfer between consecutive pairs of contacting teeth [2,7,22]. Figure 3 shows the objective parabolic function

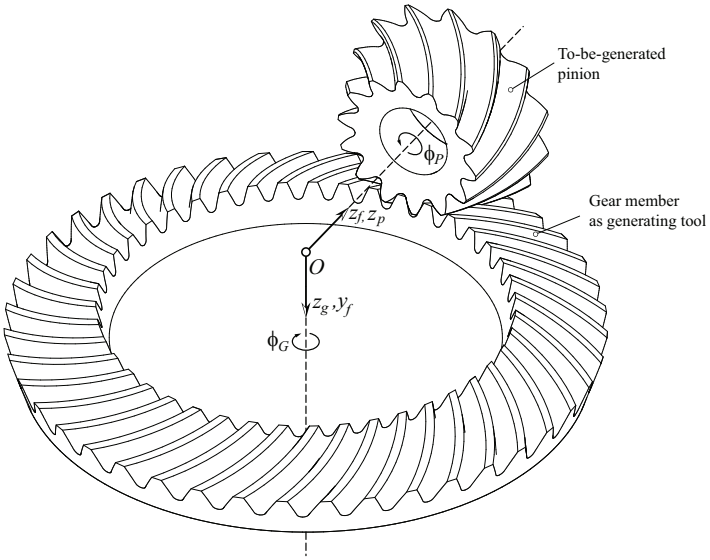

Fig. 2 Theoretical generation of a spiral bevel pinion by its mating spiral bevel gear.

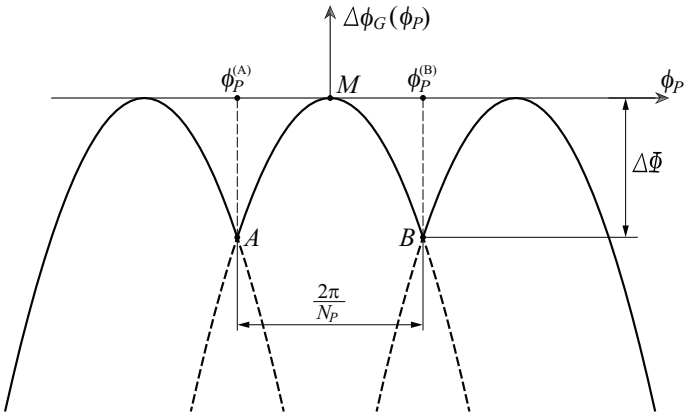

Fig. 3 Predesigned parabolic function of transmission errors.

of transmission errors, with parameter $\Delta\Phi$ representing the preset maximum level of transmission errors. The angle of rotation of the generating gear ϕ_G as a function of the angle of rotation of the pinion ϕ_P that provides the objective parabolic function of transmission errors as shown in Figure 3 is given by

$$\phi_G(\phi_P) = m_{21}\phi_P - \Delta\Phi\left(\frac{N_P}{\pi}\right)^2\left(\phi_P - \phi_P^{(M)}\right)^2 \tag{8}$$

where m_{21} is the inverse of the gear ratio of the gear set, determined as

$$m_{21} = \frac{N_P}{N_G} \tag{9}$$

with N_P and N_G being the number of teeth of the pinion and gear, respectively. Angle $\phi_P^{(M)}$ in Eq. (8) denotes the angle of rotation of the pinion during the generation of a point on the pinion tooth surface by the mean contact point M defined on the generating gear tooth surface. Because ϕ_G is a function of ϕ_P, the derivative $\partial\mathbf{r}_P(s,\theta,\phi_P,\phi_G)/\partial\phi_P$ in Eq. (7) has to take into account the derivative

of ϕ_G with respect to ϕ_P, that is obtained as

$$\frac{d\phi_G}{d\phi_P} = m_{21} - 2\Delta\Phi \left(\frac{N_P}{\pi}\right)^2 \left(\phi_P - \phi_P^{(M)}\right) \tag{10}$$

By considering the modified roll function given by Eq. (8), the generated surface of the pinion will yield a negative parabolic function of transmission errors of the considered maximum level $\Delta\Phi$ (Figure 3) during the meshing with the mating gear.

Simultaneous consideration of Equations (2), (7) and (8) allows the active surfaces of the spiral bevel pinion to be determined and represented in coordinate system $S_p\,(x_p, y_p, z_p)$, by

$$\mathbf{r}_p(s,\theta) \equiv \begin{cases} \mathbf{r}_p\,(s,\theta,\phi_P,\phi_G) = \mathbf{M}_{pg}\,(\phi_P,\phi_G)\,\mathbf{r}_g(s,\theta) \\ f_p\,(s,\theta,\phi_P,\phi_G) = 0 \\ \phi_G(\phi_P) = m_{21}\phi_P - \Delta\Phi\left(\frac{N_P}{\pi}\right)^2 \left(\phi_P - \phi_P^{(M)}\right)^2 \end{cases} \tag{11}$$

5 Determination and modification of potential contact lines

After application of Stage 2 of the proposed procedure, pinion and gear are in line contact and yield a parabolic function of transmission errors when in mesh. Figure 4 shows the results of tooth contact analysis of a pinion generated following a modified roll function as presented above and its mating gear. The contact lines cover the whole surface of pinion and gear and the function of transmission errors follows the predesigned shape and yield the maximum considered value $\Delta\Phi$. The results of tooth contact analysis represented in Figure 4 were obtained considering only one pair of teeth in contact and a rotation of the pinion corresponding to two cycles of meshing. If the angle of rotation of the pinion is extended, the successive instantaneous contact lines will cover entirely the surfaces of the pinion and wheel.

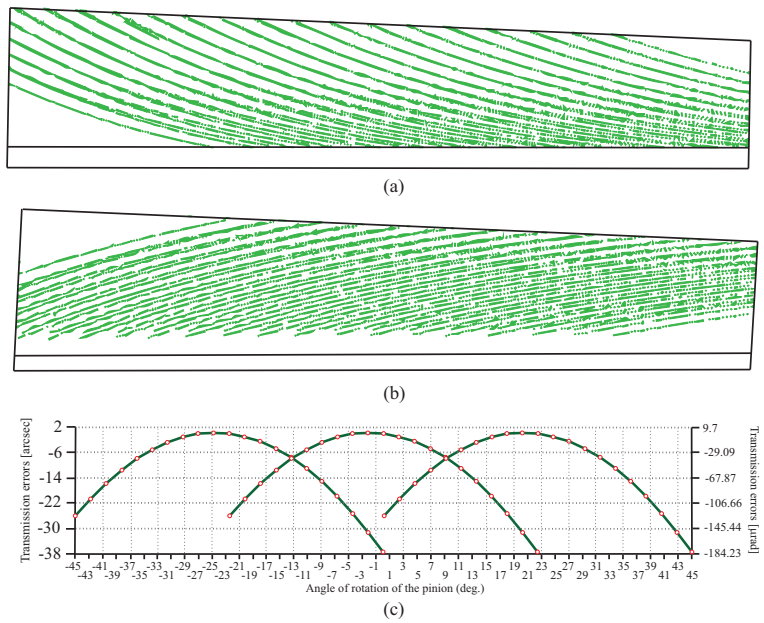

Fig. 4 Results of tooth contact analysis of a pinion with its generating mating gear wherein modified roll was applied: (a) contact lines on the pinion tooth surfaces, (b) contact lines on the gear tooth surfaces, and (c) predesigned function of transmission errors.

The pinion tooth surfaces are in line contact with its mating gear that is also its theoretical generating tool. In order to localize the contact and provide point contact (that will be extended into an elliptical contact area with the elastic deformation of pinion and gear tooth surfaces), the approach proposed in [8,9] is applied.

5.1 Orientation, positioning and sizing of the contact pattern

The desired contact path is defined on the radial projection of the pinion tooth surfaces (Figure 5). The contact path can assume any arbitrary geometrical curve although in this work, a line-type contact path will be considered. Let M be the mean contact point on the pinion active tooth surface. A coordinate system $O_r(\xi, \rho)$ with origin in point M is defined in the radial projection of the pinion tooth surface, as shown in Figure 5, with axis ξ oriented along the axis z of the pinion and axis ρ oriented in radial direction. Therefore,

$$\xi = z_p, \quad \rho = \sqrt{x_p^2 + y_p^2} \tag{12}$$

with x_p, y_p, and z_p being the coordinates of any point of the pinion tooth surfaces in coordinate system S_p fixed to the pinion. The desired contact path can be defined in coordinate system $O_r(\xi, \rho)$ by angle μ that will take into account the bias of the contact path. The following equation gives any point on the desired path by means of its coordinates ξ and ρ

$$\rho - \rho_M = -\tan(\mu)(\xi - \xi_M) \tag{13}$$

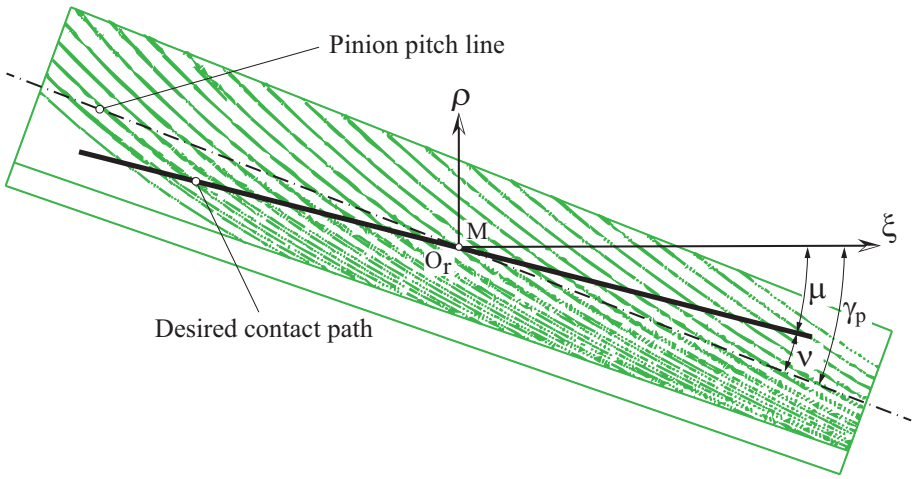

Fig. 5 Definition of the desired direction of the contact path on the radial projection of the pinion tooth surfaces.

Angle μ is given by

$$\mu = \gamma_p - \nu \tag{14}$$

being ν the bias with respect to the longitudinal direction of the contact path, defined along the pitch cone of the pinion. Angle γ_p is the pitch angle of the pinion.

A grid is now defined on the radial projection of the pinion tooth, as shown in Figure 6, with N points in profile direction and M points in longitudinal direction. Deviations on the radial projection to yield the desired dimensions of the instantaneous contact ellipses has to be computed by determining the distances from each node of the radial grid to the contact path along the potential contact lines passing through the considered node of the radial grid.

If a point P on the radial grid is located at a distance a from the desired contact path, being $2a$ the chosen length of the major axis of the instantaneous contact ellipses, the deviation of the objective surface should be equal to the virtual marking compound thickness, commonly considered equal to 0.0065 millimeters. By considering a quadratic dependence of the deviation δ on the distance d along the potential contact line, δ will be given in millimeters by

$$\delta = \frac{0.0065}{a^2} d^2 \tag{15}$$

Let us consider now a generic point P on a node of the radial grid, which will be defined by its radial projection coordinates ξ_P and ρ_P, and a generalized parameter of rotation of the pinion ϕ_P. The point of intersection P_{cp} of the potential contact line passing through point P and the contact path has to be determined, knowing that the generalized parameter of rotation of the pinion for generation of point P_{cp} is equal to ϕ_P. The condition that point P_{cp} lies on the desired contact path, given by the following equation, has to be observed:

$$\rho_{P_{cp}} - \rho_M = -\tan(\mu)(\xi_{P_{cp}} - \xi_M) \tag{16}$$

Distance between points P and P_{cp} can be approximated to be lineal along the potential contact line, and therefore the determination of the distance d will be obtained as

$$d = \sqrt{(\rho_P - \rho_{P_{cp}})^2 + (\xi_P - \xi_{P_{cp}})^2} \tag{17}$$

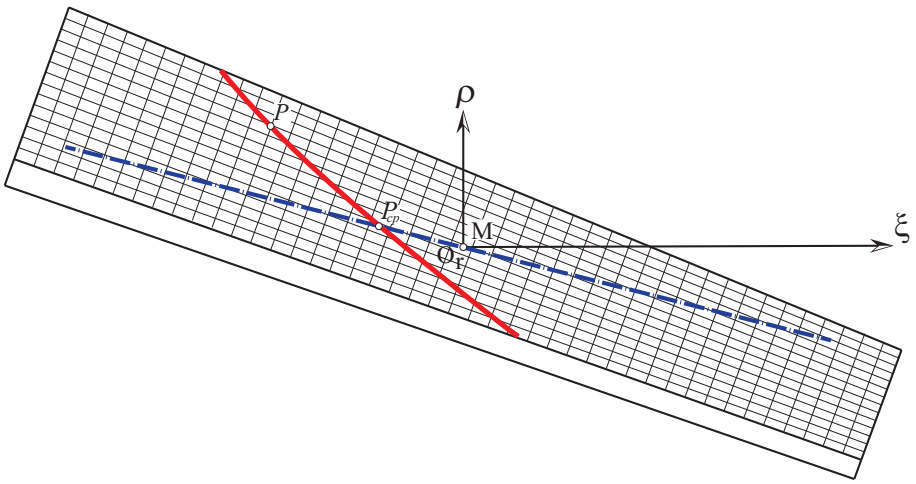

Fig. 6 Towards determination of distance between generic point P and point P_{cp} located on the desired contact path and same potential contact line.

Repeating the described procedure for all points of the radial grid, the deviations corresponding to the objective geometry of the pinion active tooth surfaces are obtained at all points of the radial grid defined on the pinion tooth surfaces. The computed deviations have to be added to the geometry of the pinion that considers the modified roll for the predesigned function of transmission errors along the normal to the surface on all points of the radial grid and in this way, the objective geometry is obtained.

6 Determination of the closest manufacturable pinion tooth surfaces

At this point, the ideal surfaces for the pinion teeth have been designed, yielding the desired contact pattern, contact path direction, and predesigned function of transmission errors. However, those surfaces have to be manufactured and for that, the machine-tool settings corresponding to the closest manufacturable tooth surfaces of the spiral bevel pinion have to be determined.

The algorithm of Levenberg-Marquardt (LM) with a trust-region strategy has been applied to minimize the deviations between the objective and the manufacturable pinion tooth contact surfaces. It consists of an iterative algorithm used in nonlinearly bound-constrained and unconstrained optimization problems in which the objective function is formulated in terms of least-squares. The LM algorithm belongs to the family of second derivative unconstrained methods, and constitutes an improvement of the Newton's method for nonlinear least-squares problems [23–27].

6.1 Definition of the optimization problem

In this optimization problem, the objective surface constitutes the spiral bevel pinion member active surface given by the final desired topography.

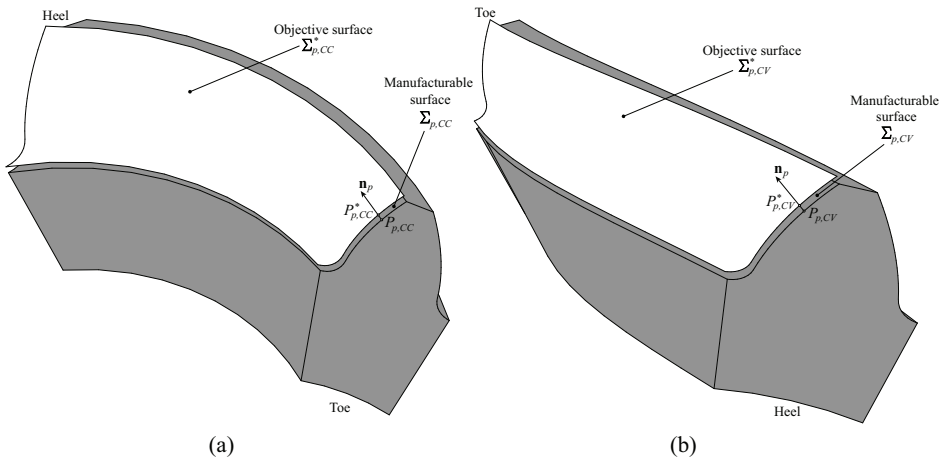

Fig. 7 Schematic representation of manufacturable surfaces and objective surfaces for the fixed-settings face-milled spiral bevel pinion: (a) tooth concave active surface; (b) tooth convex active surface.

Figure 7 shows a representation of the problem approach. Both objective tooth active surfaces have been discretized into regular numerical grids comprised of N points in profile direction and M points in lengthwise direction. The objective active surface Σ^*_p, as obtained in the previous section, will be expressed in coordinate system $S_p\,(x_p, y_p, z_p)$ by $\mathbf{r}^*_p$. Additionally, the active surface Σ_p finished through the face-milling fixed-settings cutter can be depicted in the same coordinate system by $\mathbf{r}_p(s,\theta)$, and it can be generated through the following system of nonlinear equations, similar to Equation (1):

$$\mathbf{r}_p(s,\theta) \equiv \begin{cases} \mathbf{r}_p^{(P)}(s,\theta,\psi_p) = \mathbf{M}_{pt}(\psi_p)\mathbf{r}_t(s,\theta) \\ f_p(s,\theta,\psi_p) = \left(\frac{\partial \mathbf{r}_p(s,\theta,\psi_p)}{\partial s} \times \frac{\partial \mathbf{r}_p(s,\theta,\psi_p)}{\partial \theta}\right) \cdot \frac{\partial \mathbf{r}_p(s,\theta,\psi_p)}{\partial \psi_p} = 0 \end{cases} \tag{18}$$

The normal deviations between both, the objective tooth active surface and the manufacturable active surface, Δn, can be expressed by

$$\Delta n(s,\theta) = \left(\mathbf{r}^*_p - \mathbf{r}_p(s,\theta)\right) \cdot \mathbf{n}_p(s,\theta) \tag{19}$$

where $\mathbf{n}_p(s,\theta)$ represents the unit normal vector to the manufacturable active surface and is calculated as

$$\mathbf{n}_p(s,\theta) = \frac{\frac{\partial \mathbf{r}_p(s,\theta)}{\partial s} \times \frac{\partial \mathbf{r}_p(s,\theta)}{\partial \theta}}{\left| \frac{\partial \mathbf{r}_p(s,\theta)}{\partial s} \times \frac{\partial \mathbf{r}_p(s,\theta)}{\partial \theta} \right|} \tag{20}$$

Equation (19) can be singled out for each point (i,j) belonging to the aforementioned numerical grid through the following equation

$$\Delta n_{i,j}\left(s_{i,j},\theta_{i,j}\right) = \left(\mathbf{r}_p^* - \mathbf{r}_p\left(s_{i,j},\theta_{i,j}\right)\right) \cdot \mathbf{n}_p\left(s_{i,j},\theta_{i,j}\right) \qquad \forall \begin{cases} i = 1,2,\ldots,M \\ j = 1,2,\ldots,N \end{cases} \tag{21}$$

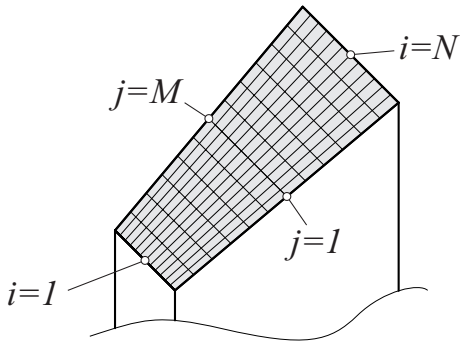

Fig. 8 Regular discretization grid of tooth active surface on radial projection.

Position vector $\mathbf{r}_p^*$ is computed at the intersection point of the normal $\mathbf{n}_p(s,\theta)$ with the objective surface pinion active tooth surface Σ_p^*. Once the deviations are computed for all points of the radial grid (Figure 8), a numerical procedure to minimize those deviations $\Delta n_{i,j}$ between the objective spiral bevel pinion active tooth surface Σ_p^* and the manufacturable surface Σ_p by a fixed-settings cutter is applied.

The first stage of the optimization process is to set up the generalized nonlinear bound-constrained optimization problem, which has been formulated in Equation (22). An objective function $f(\mathbf{x}) : \mathbb{R}^n \to \mathbb{R}$, which is laid out as sum of squares of m smooth functions $r_j(\mathbf{x}) : \mathbb{R}^n \to \mathbb{R}$ $(\forall j = 1,2,\ldots,m)$ called residuals, is required to be minimized (ideally nulled). Vector $\mathbf{r}(\mathbf{x}) = [r_1(\mathbf{x}), r_2(\mathbf{x}), \ldots, r_m(\mathbf{x})]^T : \mathbb{R}^n \to \mathbb{R}^m$ constitutes the residual vector, while vector $\mathbf{x} = [x_1, x_2, \ldots, x_n]^T \in \mathbb{R}^n$ contains the independent optimization variables. Besides, the set Ω constitutes a subset of $\mathbb{R}^n$ denominated the constraint set or feasible set.

$$\begin{cases} \text{Minimize} & f(\mathbf{x}) = \frac{1}{2}\mathbf{r}(\mathbf{x})^T\mathbf{r}(\mathbf{x}) = \frac{1}{2}\left\|\mathbf{r}(\mathbf{x})\right\|^2 = \frac{1}{2}\sum_{i=1}^{m} r_i^2(\mathbf{x}), \qquad m \geq n \\ \text{subject to} & \mathbf{x} \in \Omega \end{cases} \tag{22}$$

Next, variable vector $\mathbf{x}$, objective function $f(\mathbf{x})$, and set of constraints Ω contained in Equation (22) will be singled out for the optimization problem.

– Vector of optimization variables $\mathbf{x}$ is comprised of all or, at least, some of the machine-tool settings involved in the finishing process of the considered spiral bevel pinion active surface. Consequently, the complete variable vector is defined in (23). Furthermore, those finishing machine-tool settings not considered in the optimization process will be fixed.

$$\mathbf{x} = \left[\, \Delta X_D \; \Delta X_B \; \Delta E_m \; S_r \; q \; m_{wc} \; C \; D \; E \; r \; \alpha \; \rho \,\right]^T \tag{23}$$

Here, ΔX_D is the machine center to back, ΔX_B is the sliding base, ΔE_m is the blank offset, S_r is the radial distance, q is the cradle angle, m_{wc} is the velocity ratio, C, D and E are the modified

roll coefficients, r is the blade point radius, α is the blade profile pressure angle, and ρ is blade edge radius. A detailed description of these machine-tool settings can be found in [2].

– The objective function has been set out as the sum of squares of distances between the objective and best-fit manufacturable active surfaces measured in every point of the regular numerical grid of surface discretization. Accordingly, the objective function can be expressed through Equation (24).

$$f(\mathbf{x}) \equiv \frac{1}{2} \sum_{i=1}^{M} \sum_{j=1}^{N} \Delta n_{i,j}^2 \left(s_{i,j}, \theta_{i,j}, \mathbf{x}\right) \tag{24}$$

– The set of mathematical constraints has been established in order to avoid, firstly, deriving unreal geometric dimensions of the finishing face-milling fixed-settings cutter and, secondly, surpassing the physical limits of the hypoid gear generator. These finishing machine-tool setting constraints must simultaneously fulfil some restrictions, as follows:

$$\alpha \geq 0 \tag{25a}$$

$$r \geq 0 \tag{25b}$$

$$S_r \geq 0 \tag{25c}$$

7 Numerical example

A numerical example of design of a face-milled generated spiral bevel gear drive manufactured by the *Five-Cut Process* has been proposed in order to illustrate the proposed approach. Table 1 shows the initial design data of the reference face-milled spiral bevel gear drive.

Table 1 Initial design data of the reference face-milled spiral bevel gear drive.

Parameter	UNITS	PINION	GEAR
Reference gear ratio, u	-	2.5	
Nominal torque, T	Nm	682.09	1747.86
Rotation speed, n	rpm	1400	546.34
Shaft angle, Σ	deg.	90	

Application of *ANSI/AGMA 2005-D03* [20] and *ANSI/AGMA ISO 23509-A08* [21] standards enables to size the considered gear drive by determining blank geometry data from the initial data. Table 2 reflects both design and geometry parameters of the reference face-milled spiral bevel gear drive.

The gear finishing machine-tool settings will be derived according to the approach described in [14, 15]. As known, in a *Five-Cut Process* [28,29] the gear member is generated by means of a spread-blade face-milling cutter. Table 3 shows the finishing machine-tool settings for the generated gear member. The cutter point width P_w has been slightly increased regarding the corresponding value provided by the approach presented in [14,30] ($P_w = 2.2891$ mm) and based on the standards *ANSI/AGMA 2005-D03* [20] and *ANSI/AGMA ISO 23509-A08* [21], to reduce the gear tooth thickness and, simultaneously, allow the pinion tooth thickness and its mechanical strength to be increased. Essentially, balancing of contact stresses between pinion and gear constitutes the main reason of this decision, since, otherwise, the teeth of the pinion with standardized tooth thickness may become too narrow.

Next, the pinion finishing machine-tool settings have to be determined. In a *Five-Cut Process*, the pinion tooth surfaces are generated separately by two independent fixed-settings face-milling cutters [28,29]. The conditions of meshing and contact must be defined previously by means of the procedure described in Sections 4.3 and 5.1. Three different cases of design have been proposed in this work, whose main contact properties are shown in Table 4. In all of them, pinion concave tooth active

Table 2 Basic design and geometry parameters of the reference face-milling spiral bevel gear drive.

Design feature	UNITS	PINION	GEAR
Hand of spiral	-	Left	Right
Number of teeth, N	-	16	41
Outer pitch diameter, d_e	mm	87.6429	224.5849
Face width, b	mm	36	
Mean spiral angle, β	deg.	35	
Spread-blade cutter mean radius, r_c	mm	76.2	
Outer pitch cone distance, R_e	mm	120.5401	
Nominal design pressure angle - drive side, α_{dD}	deg.	20	
Nominal design pressure angle - coast side, α_{dC}	deg.	20	
Mean addendum factor, c_{ham}	-	0.2564	
Depth factor, k_d	-	2.0000	
Clearance factor, k_c	-	0.1250	
Thickness factor, k_t	-	0.0834	
Outer transverse module, m_{et}	mm	5.478	
Pitch cone angle, δ	deg.	21.3179	68.6821
Face cone angle, δ_a	deg.	23.6452	69.4846
Root cone angle, δ_f	deg.	20.5154	66.3548
Tooth taper	-	Duplex depth taper	
Outer addendum, h_{ae}	mm	6.4082	2.2095
Outer dedendum, h_{fe}	mm	3.1637	7.3624
Outer working depth, h_{we}	mm	8.6177	
Outer whole depth, h_e	mm	9.5719	

Table 3 Finishing machine-tool settings for the generated face-milled spiral bevel gear.

Basic machine-tool settings	UNITS	INNER BLADE	OUTER BLADE
Machine center to back, ΔX_{DG}	mm	0.0000	
Sliding base, ΔX_{BG}	mm	-2.4616	
Blank offset, ΔE_{mG}	mm	0.0000	
Radial distance, S_{rG}	mm	85.7183	
Basic cradle angle, q_G	deg.	46.7350	
Machine root angle, γ_{mG}	deg.	66.3548	
Gear roll ratio, m_{wc_G}	-	1.072562	
Spread-blade cutter mean radius, r_c	mm	76.2000	
Point width, P_w	mm	2.8000	
Profile pressure angle, α_G	deg.	21.3179	18.6441
Root fillet radius, ρ_G	mm	0.9312	0.9312
Main profile type	-	Straight	

surfaces will work as driving surfaces, whereas gear convex tooth active surfaces will be considered as driven surfaces. Accordingly, the contact properties on the pinion concave tooth active surfaces are different for each of the aforementioned design cases, while the corresponding to the pinion coast tooth active surfaces (pinion convex surfaces) are common to all of them. A similar procedure can be followed in order to get the desired contact pattern and function of transmission errors on the convex side of the pinion surfaces.

Table 4 Contact pattern design parameters at the pinion tooth surfaces.

Design parameters	UNITS	CASE 1	CASE 2	CASE 3
Concave side contact path bias regarding pitch cone, ν_{CC}	deg.	0	2	4
Concave side contact ellipse major semi-length, a_{CC}	mm	7	6.5	6
Concave side transmission error maximum level, $\Delta\Phi_{CC}$	arc sec	8	8	8
Convex side contact path bias regarding pitch cone, ν_{CV}	deg.	30	30	30
Convex side contact ellipse major semi-length, a_{CV}	mm	5	5	5
Convex side transmission error maximum level, $\Delta\Phi_{CV}$	arc sec	8	8	8

The proposed adjusted contact pattern on pinion concave tooth active surfaces for each of the proposed cases of design, together with their corresponding common function of transmission errors, are represented in Figure 9. The applied numerical algorithm to obtain the representation of the contact pattern and function of transmission errors constitutes a simulated loaded tooth contact analysis (SLTCA) approach [10], and it is based on the rigid body hypothesis of contact of mating surfaces; accordingly, no elastic tooth deformation is considered for contact pattern estimation. The contact path tracing and the numerical derivation of the function of transmission errors are based on the ideas presented by Galina I. Sheveleva [31], according to which the relative position between pairs of contacting tooth surfaces is taken into account, and the distance between them is minimized until contact is reached. Here, the algorithm of tooth contact analysis was extended to consider three pairs of contacting teeth. Contact ellipses are represented by those points which are positioned at a relative distance between mating surfaces given by a preestablished virtual marking compound thickness, usually equal to 0.0065 mm for slightly loaded gear drives.

As depicted in Figure 9, all proposed bearing contact orientations possess a slight deviation from the longitudinal direction. Besides, the function of unloaded transmission errors has a parabolic shape with a peak-to-peak maximum level of 8 arc-seconds.

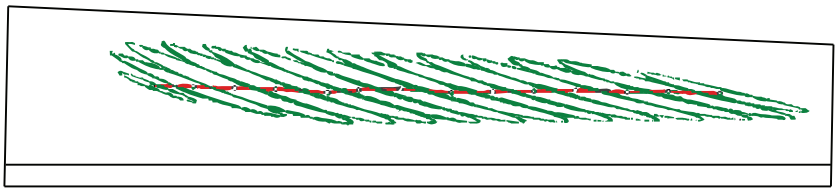

(a) Contact pattern on the concave side of the pinion tooth surfaces - CASE 1

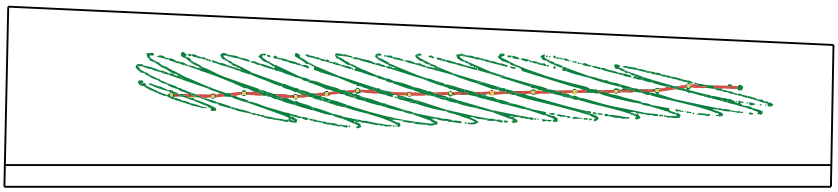

(b) Contact pattern on the concave side of the pinion tooth surfaces - CASE 2

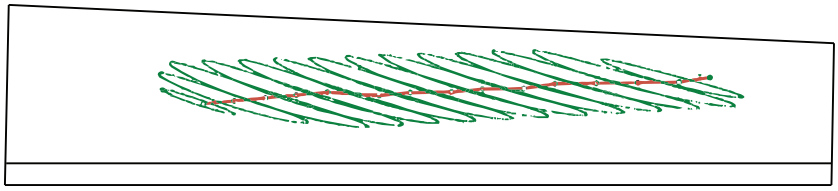

(c) Contact pattern on the concave side of the pinion tooth surfaces - CASE 3

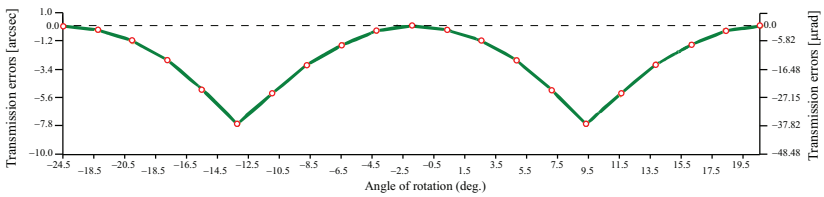

(d) Function of transmission errors

Fig. 9 Preestablished contact properties for the objective geometries.

The pinion finishing machine-tool settings required to generate the objective geometry (pinion tooth active surfaces), or, at least, approximate it as much as possible, are derived numerically through the application of the optimization procedure described in Section 6 and based on the Levenberg-Marquardt algorithm. Equation (26) represents the optimization variable vector. Pinion machine root angle γ_{mP} has been fixed, and, consequently, it remains constant throughout the optimization process. Furthermore, Table 5 contains the initial values adopted by the machine-tool settings as guess values, as well as their corresponding valid variation ranges during the optimization process, which are related with the geometry restrictions of face-milling fixed-settings cutters and the physical limits of hypoid gear generators given by Equation (25). The total number of machine-tool settings to be determined is twelve. Table 6 shows the numerical results finally derived after the mathematical optimization algorithm has converged in each design case.

$$\mathbf{x} = \left[\Delta X_{DP}\ \Delta X_{BP}\ \Delta E_{mP}\ S_{rP}\ q_P\ m_{wc_P}\ C\ D\ E\ r_P\ \alpha_P\ \rho_P \right]^T \tag{26}$$

Table 5 Initial values of machine tool settings and cutter geometry for the Levenberg-Marquardt algorithm.

Parameter	Units	Minimum Value	Initial value	Maximum Value	Fixed
Machine center to back, ΔX_{DP}	mm	- 10.0000	0.0000	10.0000	No
Sliding base, ΔX_{BP}	mm	- 10.0000	- 0.4717	10.0000	No
Blank offset, ΔE_{mP}	mm	- 10.0000	0.0000	10.0000	No
Radial distance, S_{rP}	mm	51.4512	85.7521	120.0529	No
Basic cradle angle, q_P	deg.	28.0266	46.7111	65.3955	No
Machine root angle, γ_{mP}	deg.	-	20.5007	-	Yes
Velocity ratio, m_{wc_P}	-	1.649858	2.749763	3.849668	No
Modified roll coefficient C	-	-0.10000	0.00000	0.10000	No
Modified roll coefficient D	-	-0.10000	0.00000	0.10000	No
Modified roll coefficient E	-	-0.10000	0.00000	0.10000	No
Blade profile point radius, r_P	mm	45.7200	76.2000	106.6800	No
Blade profile pressure angle, α_P	deg.	12.7907	21.3179	29.8450	No
Profile root fillet radius, ρ_P	mm	0.5587	0.9312	1.3037	No

Table 6 Finishing machine-tool settings for the generated face-milled spiral bevel pinion.

Basic machine-tool settings	UNITS	CONCAVE SIDE			CONVEX SIDE
		CASE 1	CASE 2	CASE 3	
Machine centre to back, ΔX_{DP}	mm	0.9740	0.1186	- 0.1633	7.0290
Sliding base, ΔX_{BP}	mm	- 1.4142	- 1.0851	- 0.9835	- 3.9169
Blank offset, ΔE_{mP}	mm	2.5746	3.7591	4.2944	- 10.0000
Radial distance, S_{rP}	mm	83.8497	82.4824	81.9015	97.5496
Basic cradle angle, q_P	deg.	48.4549	49.0512	48.8369	49.6452
Machine root angle, γ_{mP}	deg.	20.5154	20.5154	20.5154	20.5154
Gear roll ratio, m_{wc_P}	-	2.750173	2.705981	2.684301	3.082189
Modified roll coefficient, C	-	- 0.03098	- 0.02530	- 0.02217	- 0.01826
Modified roll coefficient, D	-	- 0.01558	0.00177	0.01000	- 0.04422
Modified roll coefficient, E	-	0.03625	0.02099	0.01678	- 0.02409
Blade profile point radius, r_P	mm	73.0663	73.3377	73.5313	77.4456
Blade profile pressure angle, α_P	deg.	18.5062	18.5037	18.6224	21.4197
Profile root fillet radius, ρ_P	mm	1.3037	1.3037	1.3037	1.3037
Main profile type	-	Straight	Straight	Straight	Straight

Contact patterns corresponding to the new derived geometries are compared with their corresponding objective geometries in Figures 10, 11, and 12. The obtained function of transmission errors for the objective geometry and the obtained manufacturable geometries are shown in Figure 13. As

illustrated, objective contact patterns are similar to the contact patterns for the manufacturable geometries obtained with the application of the Levenberg-Marquardt algorithm, since normal distances between the objective geometry and the finished-cut geometry (residual errors) are in the order of a few micrometers at worst, as depicted in Figure 14 for Case 1 (the most unfavorable situation), and, therefore, negligible regarding grinding tolerances. Consequently, the effectiveness and accuracy of the presented procedure of design of face-milled spiral bevel gear drives have been proved.

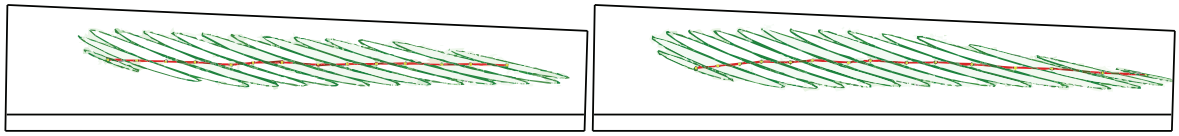

Fig. 10 Contact pattern on the concave side of the pinion tooth surfaces - CASE 1.

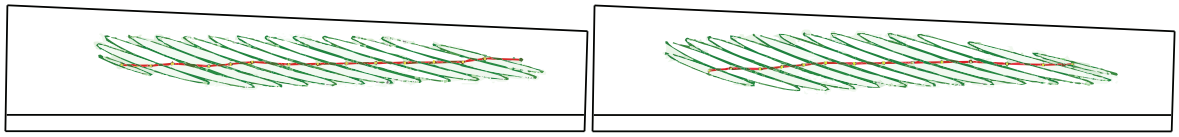

Fig. 11 Contact pattern on the concave side of the pinion tooth surfaces - CASE 2.

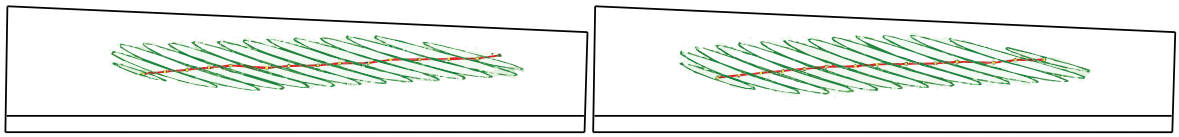

Fig. 12 Contact pattern on the concave side of the pinion tooth surfaces - CASE 3.

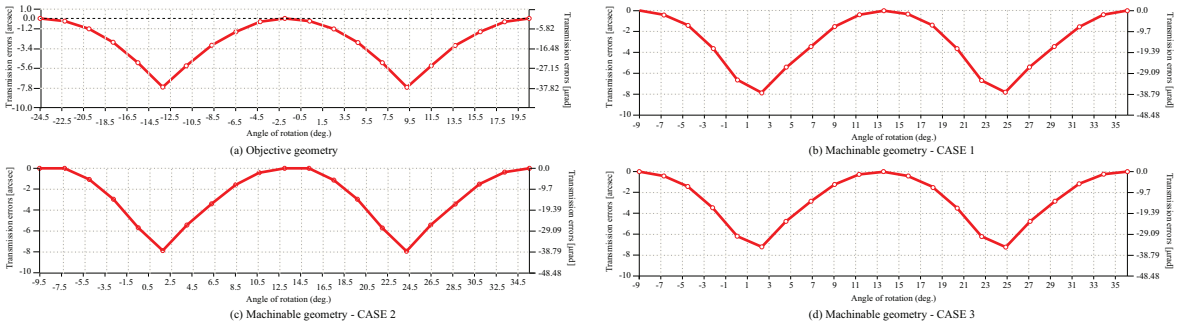

Fig. 13 Functions of transmission errors for the objective geometry and obtained manufacturable geometries.

Finite element analysis has been carried out by means of application of a general purpose computer program [32] for each of the cases of design to obtain the evolution of contact and bending stresses all over two cycles of meshing. Application of the finite element method requires the development

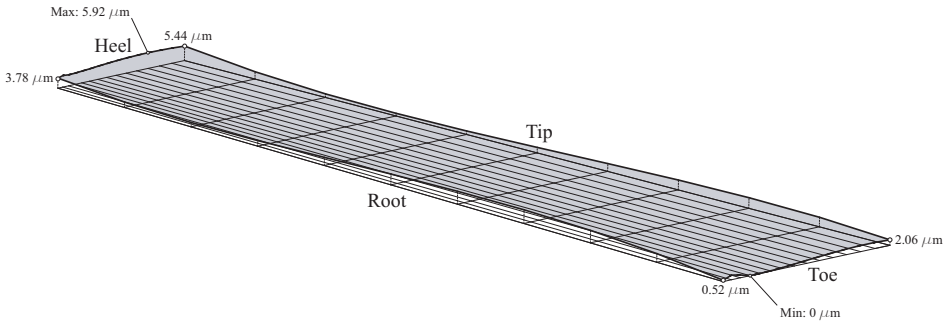

Fig. 14 Normal deviations between the objective geometry and the finished-cut geometry (CASE 1).

of finite elements models for face-milled spiral bevel gear drives, which is based on an automatic parametric computerized generation approach whose main ideas have been described in [2,5]. Finite element models are comprised of seven pairs of teeth to, firstly, ensure the independence between numerical results and boundary conditions when two consecutive cycles of meshing are analyzed, and, secondly, investigate the transference and sharing of load between contiguous pairs of teeth at simultaneous contact. Regarding the contact algorithm, the gear and pinion tooth active surfaces have been considered as master and slaves surfaces, respectively. Gear teeth and rim volumes have been meshed by means of three-dimensional continuum elements type C3D8I, which basically constitute hexahedral first-order stress/displacement elements enhanced by incompatible deformation modes in order to improve their bending behavior [32]. A linear isotropic elastic steel with general properties of elastic modulus $E = 210$ GPa and Poisson ratio $\nu = 0.30$ has been selected as the material for pinion and gear. The generated finite elements models are comprised of 103124 elements with 127622 nodes.

The evolution of the pinion Von Mises equivalent contact and bending stresses throughout two whole cycles of meshing is shown in Figure 15. A perfect uniform evolution of contact stresses is observed for Case 2, whereas some areas of higher contact stresses are detected on Cases 1 and 3 in some contact positions, although the maximum values are still acceptable. As far as bending stresses are concerned, it is visible that the lower contact pattern bias is, the higher the maximum bending stress is, although bending stresses are approximately in the same order of magnitude for all cases of design.

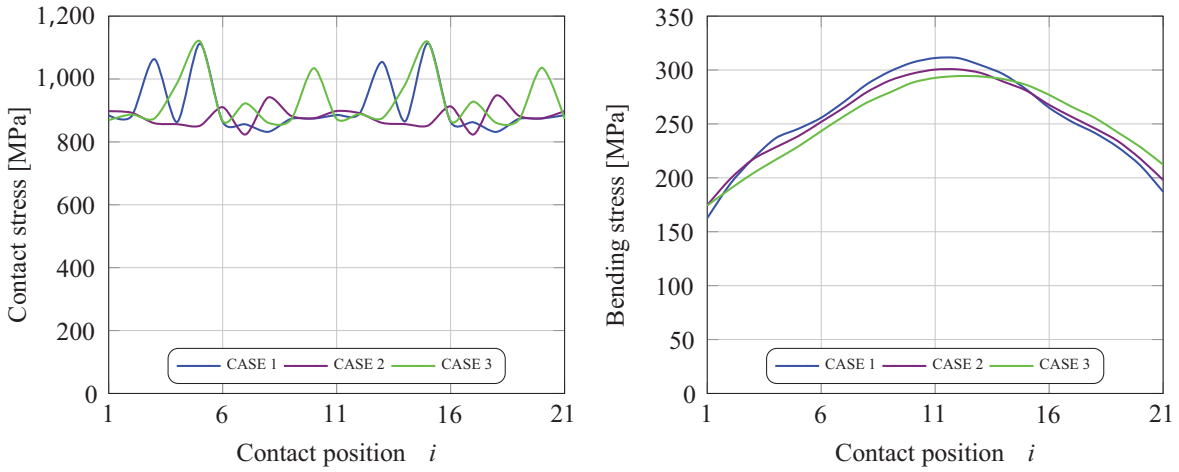

Fig. 15 Evolution of contact stresses (left) and bending stresses (right) corresponding to the face-milled spiral bevel pinion.

Figure 16 represents the evolution of Von Mises contact and bending stresses for the gear throughout two cycles of meshing. Uniform evolutions are observed in contact stresses in all cases of design. The geometry corresponding to Case 2 constitutes the best design from the mechanical behavior point of view.

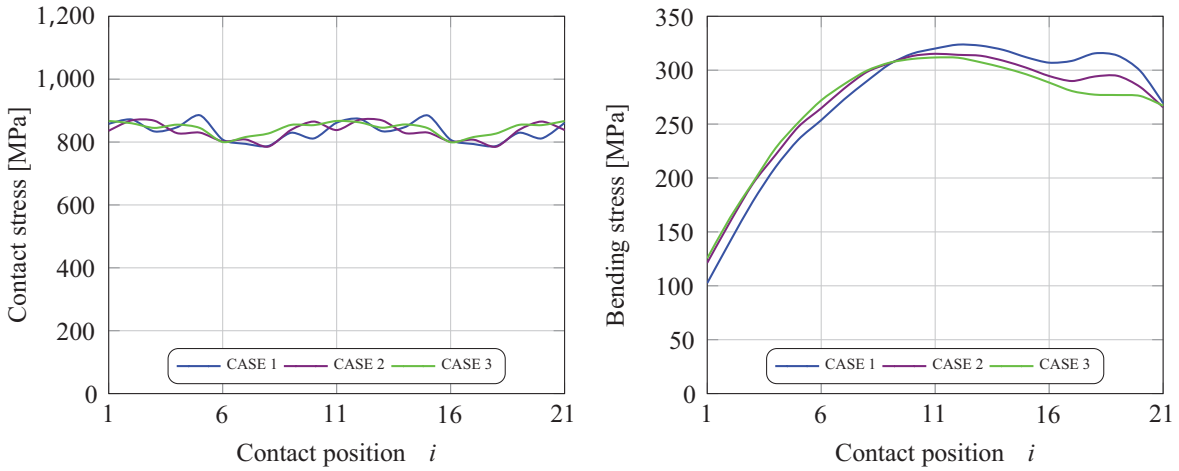

Fig. 16 Evolution of contact stresses (left) and bending stresses (right) corresponding to the face-milled spiral bevel gear.

Figures 17 and 18 show contact stresses for Cases 1 and 2 in which load transfer between contiguous pairs of contacting teeth takes place. As shown, two pairs of teeth are in mesh simultaneously.

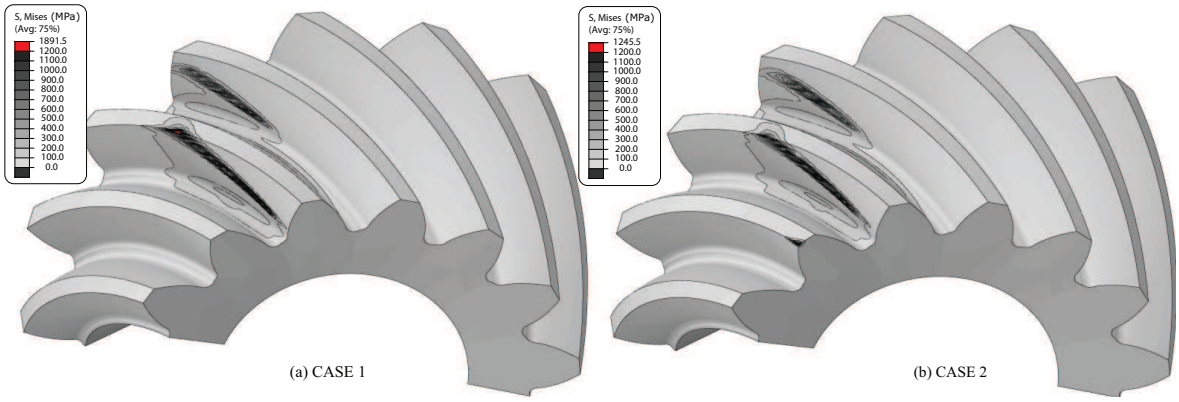

Fig. 17 Contact stresses at contact position 5 on the pinion tooth surfaces.

8 Conclusions

Based on the performed research work, the following conclusions can be drawn:

1. An integrated computerized approach of design, generation, and stress analysis of low-noise high-endurance face-milled spiral bevel gear drives machined by means of a *Five-Cut Process* has been proposed. It is based on the definition of an objective surface topography for the pinion driving active surface that takes into account a predesigned function of transmission errors with a preset

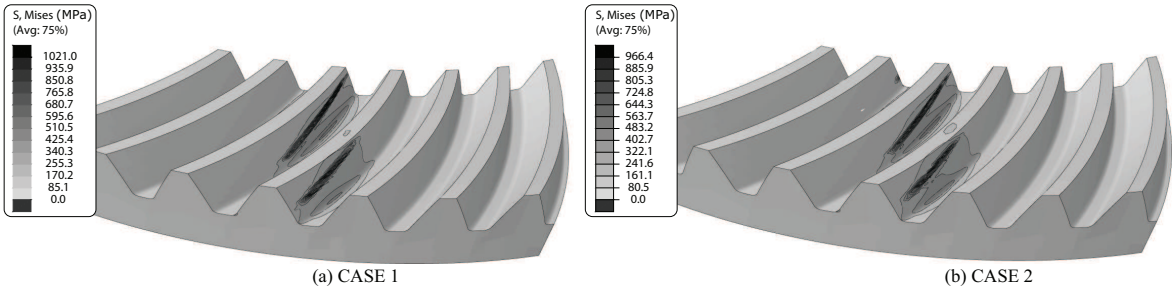

Fig. 18 Contact stresses at contact position 5 on the gear tooth surfaces.

maximum value of peak-to-peak transmission errors, a preestablished direction of the contact path and length of contact ellipses. Machine tool settings of the closest manufacturable pinion tooth surfaces are obtained by application of a bound-constrained optimization algorithm.
2. Favorable contact properties (contact pattern and a predesigned negative parabolic function of transmission errors with limited magnitude) and uniform evolution of contact and bending stresses throughout the whole cycle of meshing are obtained by the proposed approach.
3. The proposed approach has been applied to the design of a face-milled generated spiral bevel gear drive and the effectiveness and accuracy of the method shown.
4. The developed approach can be extended to the design of face-hobbed spiral bevel gear drives and/or hypoid gear drives.

Acknowledgments and compliance with ethical standards

The work of the second author has been funded by the FPI scholarship ref. BES-2011-045995 granted by the Spanish Ministry of Economy and Competitiveness (MINECO). First and third author declare that they have no conflict of interest.

References

1. S. Gear, S. T. Committee, Gear design, manufacturing and inspection manual, No. 15 in AE (Series), Society of Automotive Enginners (SAE), 1990, Ch. 9.
2. F. L. Litvin, A. Fuentes, Gear Geometry and Applied Theory, 2nd Edition, Cambridge University Press, 2004.
3. F. L. Litvin, A. Fuentes, K. Hayasaka, Design, manufacture, stress analysis and experimental tests of low-noise high endurance spiral bevel gears, Mechanism and Machine Theory 41 (1) (2006) 83–118.
4. S. P. Radzevich, Dudley's Handbook of Practical Gear Design and Manufacture, 2nd Edition, CRC Press, 2012.
5. J. Argyris, A. Fuentes, F. L. Litvin, Computerized integrated approach for design and stress analysis of spiral bevel gears, Computer Methods in Applied Mechanics and Engineering 191 (11–12) (2002) 1057–1095.
6. P.-Y. Wang, Z.-H. Fong, Adjustability improvement of face-milling spiral bevel gears by modified radial motion (MRM) method, Mechanism and Machine Theory 40 (1) (2005) 69–89.
7. P.-Y. Wang, Z.-F. Fong, Fourth-order kinematic synthesis for face-milling spiral bevel gears with modified radial motion (MRM) correction, Journal of Mechanical Design, Transactions of the ASME 128 (2) (2006) 457–467.
8. Y.-P. Shih, Z.-H. Fong, Flank modification methodology for face-hobbing hypoid gears based on ease-off topography, Journal of Mechanical Design, Transactions of the ASME 129 (12) (2007) 1294–1302.
9. Y.-P. Shih, A novel ease-off flank modification methodology for spiral bevel and hypoid gears, Mechanism and Machine Theory 45 (8) (2010) 1108–1124.
10. A. Artoni, A. Bracci, M. Gabiccini, M. Guiggiani, Optimization of the loaded contact pattern in hypoid gears by automatic topography modification, Journal of Mechanical Design, Transactions of the ASME 131 (1), 2009.
11. A. Artoni, A. Kolivand, M. Kahraman, An ease-off based optimization of the loaded transmission error of hypoid gears, Journal of Mechanical Design, Transactions of the ASME 132 (1), 2010.
12. M. Gabiccini, A. Bracci, M. Guiggiani, Robust optimization of the loaded contact pattern in hypoid gears with uncertain misalignments, Journal of Mechanical Design, Transactions of the ASME 132 (4), 2010.
13. A. Artoni, M. Gabiccini, M. Guiggiani, A. Kahraman, Multi-objective ease-off optimization of hypoid gears for their efficiency, noise, and durability performances, Journal of Mechanical Design, Transactions of the ASME 133 (12), 2011.

14. I. Gonzalez-Perez, A. Fuentes, K. Hayasaka, Analytical determination of basic machine-tool settings for generation of spiral bevel gears from blank data, Journal of Mechanical Design, Transactions of the ASME 132 (10), 2010.
15. I. Gonzalez-Perez, A. Fuentes, R. Ruiz-Orzaez, An approach for determination of basic machine-tool settings from blank data in face-hobbed and face-milled hypoid gears, Journal of Mechanical Design, Transactions of the ASME 137 (9), 2015.
16. F. L. Litvin, C. Kuan, J. C. Wang, R. F. Handschuh, J. Masseth, N. Maruyama, Minimization of deviations of gear real tooth surfaces determined by coordinate measurements, Journal of Mechanical Design, Transactions of the ASME 115 (4) (1993) 995–1001.
17. C.-Y. Lin, C.-B. Tsay, Z.-H. Fong, Computed-aided manufacturing of spiral bevel and hypoid gears by applying optimization techniques, Journal of Materials Processing Technology 114 (1) (2001) 22–35.
18. Q. Fan, R. S. DaFoe, J. W. Swanger, Higher-order tooth flank form error correction for face-milled spiral bevel and hypoid gears, Journal of Mechanical Design, Transactions of the ASME 130 (7), 2008.
19. A. Artoni, M. Gabiccini, M. Kolivand, Ease-off based compensation of tooth surface deviations for spiral bevel and hypoid gears: only the pinion needs corrections, Mechanism and Machine Theory 61 (2013) 84–101.
20. American Gear Manufacturers Association, ANSI/AGMA 2005-D03: Design manual for bevel gears, September 2003.
21. American Gear Manufacturers Association, ANSI/AGMA ISO 23509-A08: Bevel and Hypoid Gear Geometry, May 2008.
22. H. J. Stadtfeld, U. Gaiser, The ultimate motion graph, Journal of Mechanical Design, Transactions of the ASME 122 (3) (2000) 317–322.
23. P. E. Gill, W. Murray, M. H. Wright, Practical Optimization, Academic Press, 1997.
24. J. Nocedal, S. J. Wright, Numerical Optimization, Springer Series in Operations Research, Springer, 1999.
25. A. Artoni, M. Gabiccini, M. Guiggiani, Nonlinear identification of machine settings for flank form modifications in hypoid gears, Journal of Mechanical Design, Transactions of the ASME 130 (11), 2008.
26. E. K. P. Chong, S. H. Zak, An introduction to optimization, 3rd Edition, Series in discrete mathematics and optimization, John Wiley & Sons, 2008.
27. M. Gabiccini, A. Artoni, M. Guiggiani, On the identification of machine settings for gear surface topography corrections, Journal of Mechanical Design, Transactions of the ASME 134 (4), 2012.
28. H. J. Stadtfeld, Advanced bevel gear technology: manufacturing, inspection and optimization; Collected publications, The Gleason Works, 2000.
29. T. Maiuri, Spiral bevel and hypoid gear cutting technology update, Gear Technology 24 (5) (2007) 28–39.
30. I. Gonzalez-Perez, V. Roda-Casanova, A. Fuentes, Modified geometry of spur gear drives for compensation of shaft deflections, Meccanica 50 (7) (2015) 1855–1867.
31. G. I. Sheveleva, A. E. Volkov, V. I. Medvedev, Algorithms for analysis of meshing and contact of spiral bevel gears, Mechanism and Machine Theory 42 (2) (2007) 198–215.
32. ABAQUS/Standard User's Manual, Providence, Rhode Island 02909-2499 (US) (2010).